Computer-Aided Diagnosis and Quantification in Chest CT

Jin Mo Goo

Abstract

With the advances of CT and computer technology, various applications for computer-aided diagnosis (CAD) and quantification have been developed to enhance the performance of radiologists. CAD provides tools to detect more nodules, to determine nodule malignancy by characterizing and measuring nodules, and to match nodules in follow-up studies. These applications will play an important role in the nodule management for lung cancer screening with low-dose CT. Parenchymal and airway lesions in chronic obstructive lung disease and diffuse interstitial lung disease can be characterized and quantified semiautomatically and this information can be used in phenotyping of disease, in explaining functional changes, and in clinical trials. However, users need to understand the limitations and measurement variability of these approaches.

1 Introduction

CT plays a critical role in morphologic analyses of various pulmonary diseases which have been traditionally based on visual and qualitative assessment. With the advances of CT and digital technology, numerous post-processing techniques are now being applied in lesion detection, characterization, and quantification as well as three-dimensional visualization. These can be attributed to isotropic imaging of CT and easy access to digital images with the advent of picture archiving and communication systems (PACS). These valuable data provided by computer applications can enhance radiologists' performance, but the current status is far from fully automated diagnosis by computer technology. Therefore, the basic concept of computer-aided diagnosis (CAD) is to provide a computer output as a "second opinion" to assist radiologists' image interpretations (Doi et al. 1992).

CAD and quantification have been under active research in many pulmonary diseases, but this chapter will mainly focus on the applications in the evaluation of lung nodule, chronic obstructive lung disease (COPD), and diffuse interstitial lung disease (DILD).

J.M. Goo, MD, PhD
Department of Radiology, Seoul National University Hospital, 101 Daehak-ro, Jongno-gu, Seoul 03080, South Korea
e-mail: jmgoo@snu.ac.kr

2 Basic Technologic Architectures of CAD

As detailed technologic description of CAD is beyond the scope of this chapter, only basic architectures of CAD will be introduced here, which share some approaches in the evaluation of lung nodule, COPD, and DILD.

2.1 Segmentation of the Lung

The first step for lung CAD is the segmentation of the lung from other structures such as the chest wall and the mediastinum. If the lungs exhibit minimal or no pathologic conditions, this process is relatively easy compared to the segmentation of other organs such as the liver because the attenuation value of the lung is quite different from the surrounding structures. However, when a pathologic condition such as fibrosis or pleural effusion is present, the segmentation of the lung fails to perform efficiently. As no single segmentation method can achieve an optimal performance for all disease conditions at the moment, specialized methods are applied for particular disease subsets. Recent methods can also permit segmentation of lobes to compute lobar volume and parenchymal abnormalities such as areas of low attenuation (Fig. 1).

2.2 Detection of the Region of Interests

After segmenting the lung, the region of interests (ROIs) are identified, which is dependent on target of lesions: lung nodule, low attenuated pixels in the lung, airways, and typical patterns of interstitial lung disease (ILD) such as areas of ground-glass opacity (GGO), reticular opacity, nodular opacities, honeycombing, and consolidation.

The initial nodule candidates can be identified by applying a gray-level thresholding technique or shape filters to CT images. In dealing with DILD, the areas of specific patterns on CT are usually identified by machine learning-based methods. In this method, the abnormalities are predicted on the basis of the features extracted from the data.

2.3 Feature Analysis and Reduction of False-Positives

A number of image features on ROIs such as morphology (size, circularity, etc.), gray level, and texture are quantified, and false-positive findings are removed by classifiers. Linear discriminant analysis, rule-based classifier, and artificial neural network are examples of feature-based
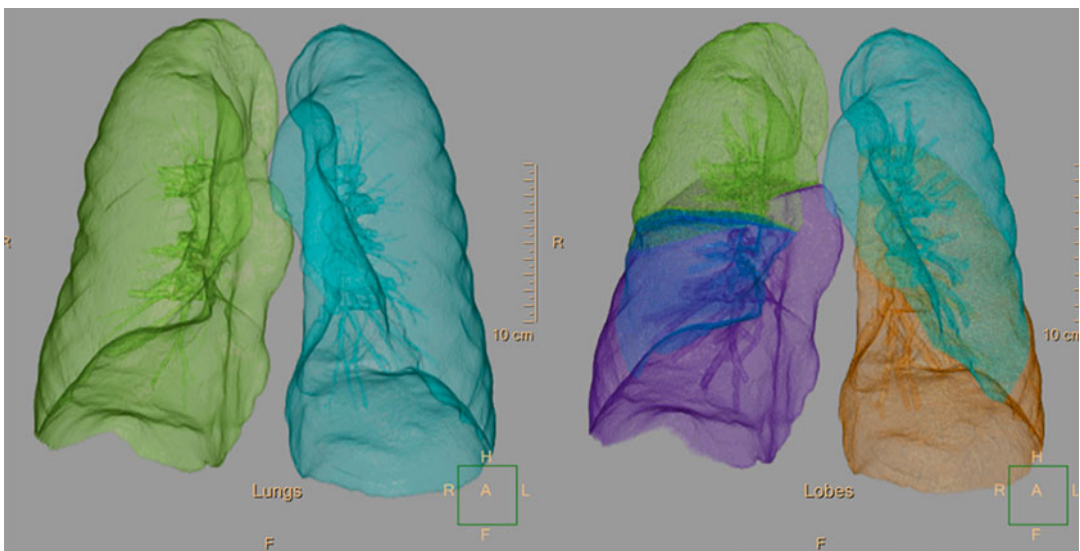

Fig. 1 Segmentation results of the lung (*left*) and each lobe of the lung (*right*)

classifiers. A classifier is trained with sets of input features and corrects class labels.

2.4 Quantification and Characterization

After segmenting ROIs from the background, various features of ROIs such as volume (Fig. 2), mass, and texture can be calculated by using the number of voxels, attenuation of voxels, and a relationship with surrounding voxels.

3 Lung Nodule

With the introduction of multidetector CT (MDCT), radiologists need to interpret a large number of CT images that require additional time and effort. Low-dose CT has been reported as an effective modality for lung cancer screening but the interpretation of low-dose CT for screening is typically a repetitive and burdensome task. As many nodules detected on screening CT are false-positives for malignancy, characterization of nodules to determine malignancy is crucial. Size, shape, and volume-doubling time of nod-

Fig. 2 Segmentation of GGN shows various measures of volume, diameter, and density

ules are well-established indicators of nodule malignancy. However, there is considerable variability in visual assessment and manual measurement in the management of nodules. Therefore, CAD can be used in the detection, measurement, and monitoring of nodules in lung cancer screening and has been employed in some clinical trials (van Klaveren et al. 2009).

3.1 Detection

3.1.1 Performance of CAD

Many studies have shown that CAD could improve radiologists' performance in detecting lung nodules but reported performance of CAD systems is variable (Goo 2011). In addition to the CAD performance itself, the results of CAD performance can be affected by the reference standard and the characteristics of evaluated datasets. The Lung Image Database Consortium (LIDC) has shown that substantial variability exists across experienced radiologists in the task of lung nodule identification (Armato et al. 2004). In this study, the mean radiologist nodule detection sensitivities ranged from 51.0 to 83.2 % with mean false-positive rates from 0.33 to 1.39 per case by applying different reference standards. To overcome this limitation in comparing CAD algorithms, a comparative study where many CAD systems are applied to the same dataset has been performed (van Ginneken et al. 2010). When a database of same 50 CT scans from a lung cancer screening trial was tested, six algorithms showed sensitivities ranging from 24.6 to 71.2 % at a false-positive rate of 2 per case and sensitivities ranging from 12.7 to 57.0 % at a false-positive rate of 0.5 per case. Interesting suggestion of this study is that the combination of six algorithms is able to achieve a sensitivity of 79.2 % at a false-positive rate of 2 per case and a sensitivity of 63.8 % at a false-positive rate of 0.5 per case which are far superior to the sensitivity of each algorithm.

The value of CAD in improving radiologists' detection performance is attributed to the fact that a CAD system performs nodule detection task differently than radiologists do. Several studies have shown that a CAD system was good
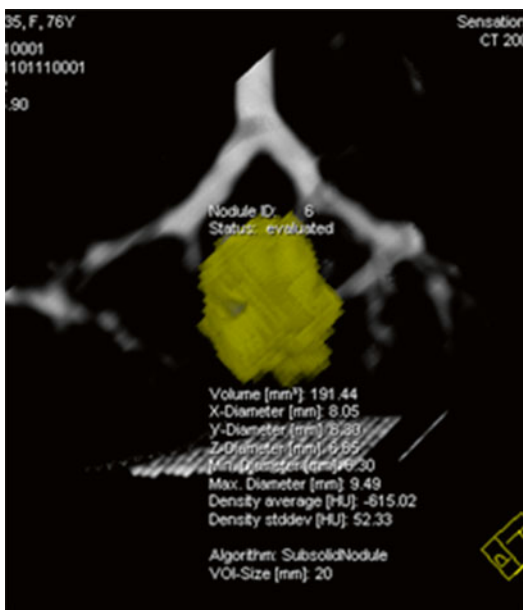
at detecting isolated and small nodules, while radiologists are good at detecting attached and relatively larger nodules (Lee et al. 2004; Marten et al. 2005). This complementary role of a human reader and CAD in detecting lung nodules may be translated into better combined performance of readers with CAD than that of a double reading. Rubin et al. showed that the sensitivity of a reader with CAD at a false-positive rate of three can be substantially higher that with a double reading (Rubin et al. 2005). In another study, when the performance of CAD was compared with that of doubling reading with a total of 400 low-dose CT, the sensitivity of nodule detection was 78.1 % for double reading and 96.7 % for CAD (Zhao et al. 2012). In this study, 21.9 % of 151 findings that needed further evaluation were missed by readers and detected by CAD only.

The early CAD programs only targeted the detection of solid nodules, but with the increase of clinical significance of subsolid nodules, many CAD programs are now equipped with the capability to detect subsolid nodules. An initial study by Kim et al. which employed texture features and Gaussian curve fitting features showed a sensitivity of 94.3 % and a positive predictive value of 29.1 % at ROI-based analysis (Kim et al. 2005). In a study by Yanagawa et al., the figure-of-merit values with CAD did not show significant differences in detecting pure ground-glass nodule (GGN) or part-solid nodules while they showed significant improvement in detecting overall and solid nodules (Yanagawa et al. 2009). These results may be caused by poor sensitivity of CAD system (21 %) compared with that of readers (60–80 %). When a CAD system with better sensitivities (95 % for part-solid nodules and 71 % for pure GGNs) was used, readers' sensitivities were significantly increased in detecting part-solid nodules from 81 to 97 % and in detecting pure GGNs from 69 to 82 % (Godoy et al. 2013).

3.1.2 Reading Mode of CAD

According to the timing of viewing the CAD results, the reading mode of CAD can be divided into first reader, concurrent reader, and second reader. In a first-reader mode, readers review the CAD-detected nodules only. As the sensitivity of CAD is not good enough at the moment, readers may miss many significant nodules, and therefore this approach is not accepted. In a concurrent-reader mode, readers assess CT images and identify nodules while the CAD results are being displayed. This approach can be time efficient, but some nodules can be missed especially when readers are dependent on CAD results. Currently, second-reader mode is the accepted approach where readers review the CAD results after readers initially read CT images without CAD results.

Two studies have compared concurrent-reader mode and second-reader mode in the usage of CAD. In a study by Beyer et al. (2007), the sensitivity in detecting nodules above 4 mm was 68 % without CAD, 68 % with CAD as a concurrent reader, and 75 % with CAD as a second reader. In terms of reading time, concurrent reading (274 s) was significantly better than reading without CAD (294 s) and using CAD as a second reader (337 s). In a study by Matsumoto et al. (2013), the detection performance was not significantly different between the concurrent-reader mode and second-reader mode (figure of merit, 0.70 and 0.72), while reading time was significantly shorter with the concurrent-reader mode (132 s) than with second-reader mode (210 s).

3.2 Nodule Volumetry

Doubling time has been used in predicting nodule malignancy, but in dealing with subcentimeter nodules detected on CT scans, manual measurements can show considerable measurement variability. After the introduction by Yankelevitz et al. who showed all five malignant nodules out of 13 nodules had doubling time less 177 days (Yankelevitz et al. 2000), the computer-aided volumetry has become an important tool in nodule management (Fig. 3).

3.2.1 Measurement Variability

At an early study, the measurement error of volumetry was reported to be as small as 3 % when evaluated with a phantom (Yankelevitz et al. 2000). Subsequent studies have shown that various
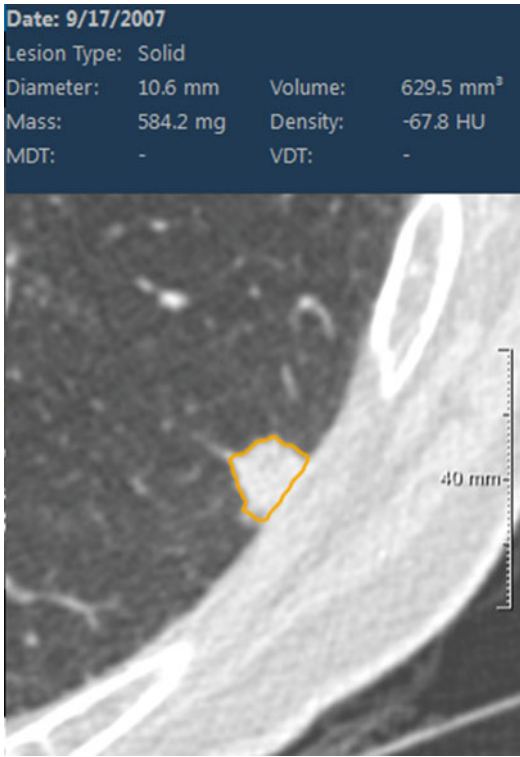
Date: 9/17/2007

Lesion Type: Solid

Diameter: 10.6 mm   Volume: 629.5 mm³

Mass: 584.2 mg   Density: -67.8 HU

MDT: -   VDT: -

40 mm

Fig. 3 Segmentation result of pleural-attached nodule showing volume of a nodule

factors can affect the measurement of nodule volume: the size and characteristics of nodules, the scan and reconstruction factors of the CT examinations, and the patient-related factors such as the respiratory status (Goo 2011; Goo et al. 2005, 2006) (Fig. 4). Volume measurements of smaller nodules, nodules attached to surrounding structures, and those with thicker CT section thickness may result in larger errors. When six software packages were compared in the evaluation of solid nodule volume, adequate segmentation determined by visual assessment could be achieved in 71–86 % of nodules, and systematic volume differences were present in 11 out of 15 comparisons (de Hoop et al. 2009). Therefore, for nodule volumetry, obtaining CT scans with thin volumetric data is essential and same software package should be used in the evaluation of interval change of nodule volume. To exclude the erroneous segmentation of nodules, readers always need to review the segmentation results as well.

As the establishment of ground truth of nodule volume in in vivo study is not feasible, the reproducibility in measuring nodule volume is more important than accuracy in determining the growth of a nodule. To evaluate the measurement variability, a same-day repeat CT protocol has been employed. After the initial study by Wormanns et al. which showed that the 95 % limits of agreement between the repeat CT scans were −20 to 22 % (Wormanns et al. 2004), many studies have shown that these limits can be up to 26 % (Goo 2011). Based on this results, the growth of a nodule in the NELSON (Nederlands-Leuvens Longkanker Screenings Onderzoek) trial was defined as an increase in nodule volume of at least 25 % between the two scans. Therefore, the measurement difference up to this threshold can be regarded as measurement error, while the measurement difference greater than this threshold can be true change between two CT scans.

3.3 Quantification of Subsolid Nodule

Due to the low contrast to the lung of subsolid nodules compared with solid nodule, segmentation of subsolid nodule is a difficult task. When a measurement error was estimated with simulated GGNs of various attenuation values, the average of the relative volume measurement error ranged from 51.1 to 85.2 % for 3 mm GGNs and from −4.1 to 7.1 % for 5 mm GGNs (Oda et al. 2010).

In addition to increased size of volume, subsolid nodules may show other growth patterns. They can show increase in attenuation, newly appeared or increased solid component, or decrease in overall size with increased solid component. To reflect these growth patterns, a measure of mass has been devised which can be calculated by multiplying nodule volume with nodule attenuation (Fig. 5). In a study by de Hoop et al., mass showed less variability and less mean time, required in determining growth than diameter or volume, which indicates that mass measurements can enable the detection of growth of subsolid nodules earlier than volume or diameter measurements (de Hoop et al. 2010). When the
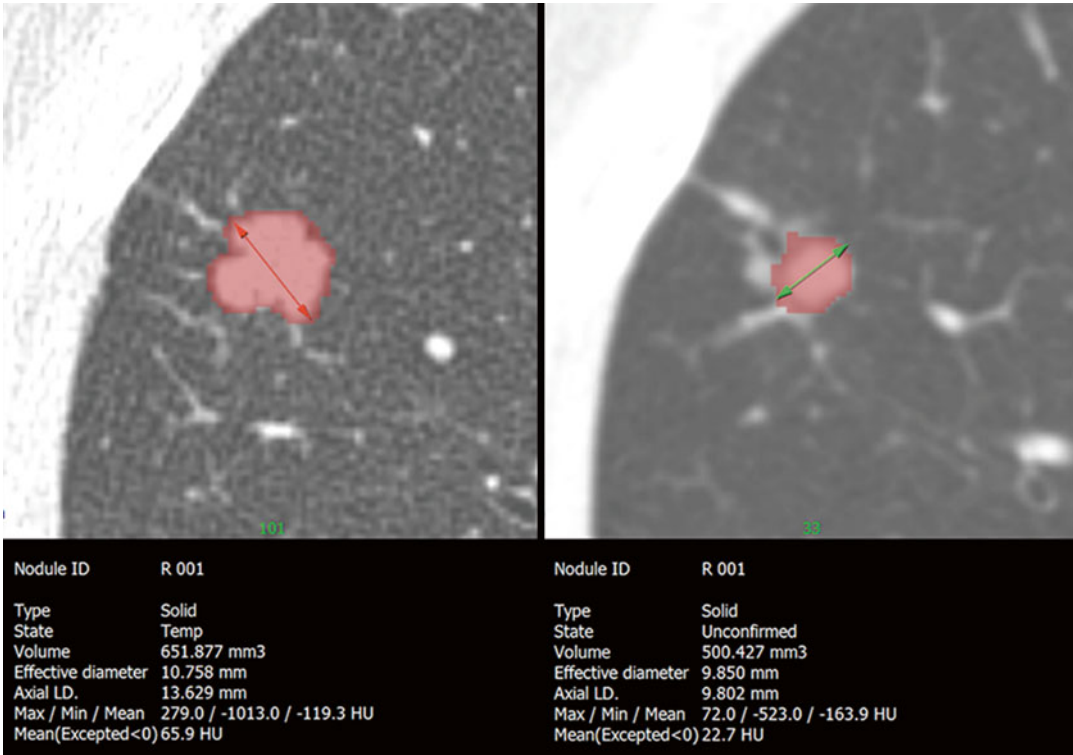
Fig. 4 CT scans of 1 mm section thickness (*left*) and 3 mm section thickness (*right*) obtained from the same raw CT data result in 26 % difference in nodule volume measurements

interscan variability of volume and mass measurement of GGN was assessed with a same-day repeat CT study, they were reported to be up to 19 % (Kim et al. 2013).

In the staging of lung adenocarcinoma, it has been suggested that the size T factor should be adjusted only to the invasive component pathologically in invasive tumors with lepidic areas. In a CT-pathology correlation study, the size of the solid component in subsolid nodules on CT has a significant correlation with the invasive component of lung adenocarcinoma on pathology (Lee et al. 2014). In an attempt to segment the solid component in subsolid nodules, a threshold of −300 HU demonstrated a good sensitivity (90 %) and specificity (88 %) (Scholten et al. 2015) (Fig. 6).

3.4 Nodule Characterization

The likelihood of nodule malignancy has been determined by experienced radiologists' visual assessment mainly based on morphology and internal composition of a nodule. Various nodule features can be quantitated according to the shape of the nodule such as sphericity and the internal configuration of the nodule such as mean attenuation or homogeneity. CAD output generated with this process may be used in determining nodule malignancy. In a study by Awai et al., the use of CAD output generated from 56 morphologic features and two clinical datasets improved the diagnostic performance of residents for the assessment of nodule malignancy while it did not improve that of radiologists (Awai et al. 2006). Texture analysis, which uses attenuation values of each voxel and their distribution within target lesions, can also provide a quantitative imaging analysis tool (Fig. 7). This approach has been applied to categorize lung adenocarcinoma manifested as subsolid nodules. In a study by Chae et al., higher kurtosis and smaller mass are significant predictors of preinvasive lesions from invasive adenocarcinomas (Chae et al. 2014).
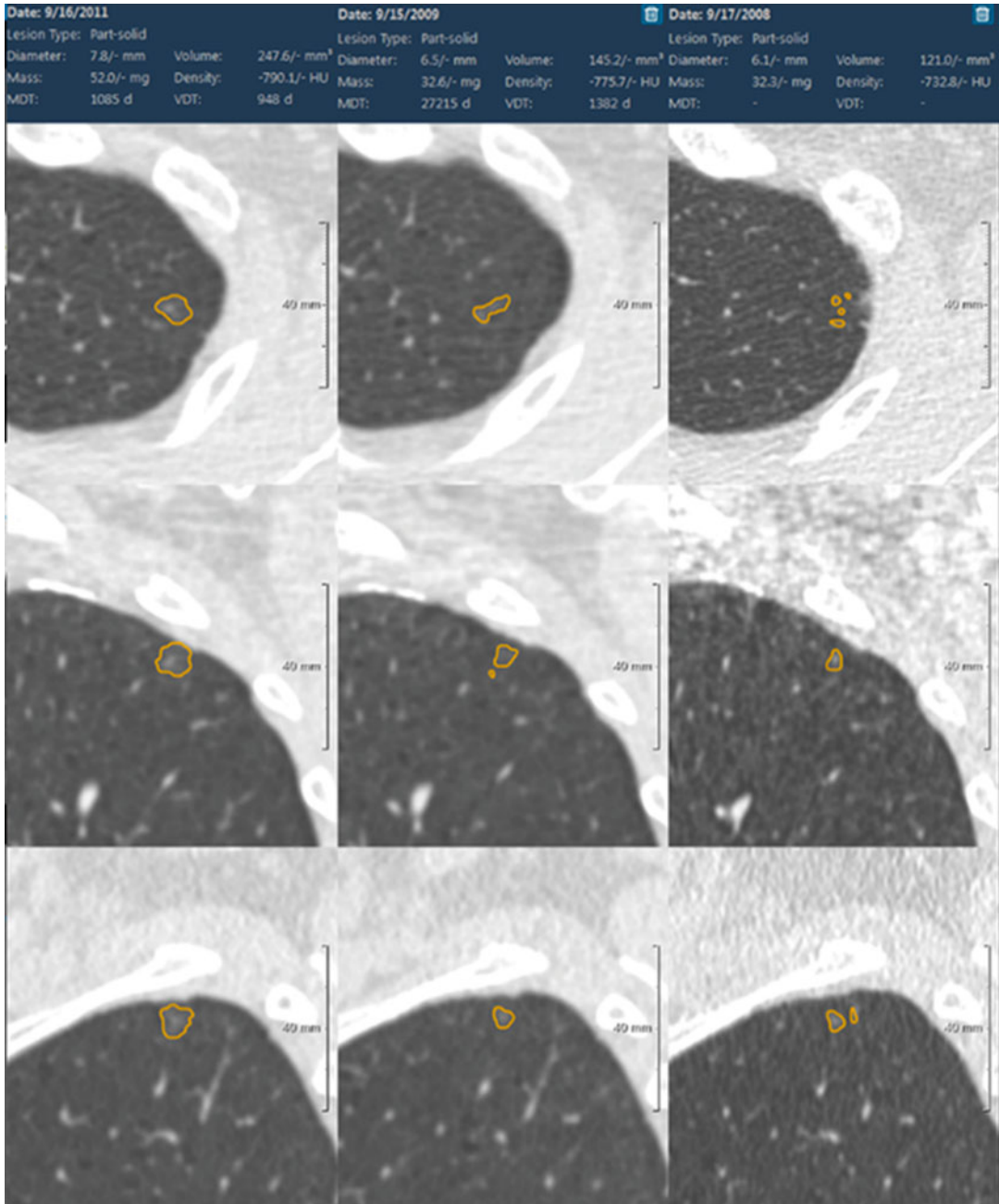
Fig. 5 Serial CT scans of a subsolid nodule show increase in diameter, volume, and mass of subsolid nodule

Similar attempt to differentiate invasive adenocarcinoma from preinvasive or minimally invasive adenocarcinoma showed that the 75th percentile CT attenuation value and entropy are predictors for invasive adenocarcinoma (Son et al. 2014).

3.5 Nodule Matching in Follow-Up CT

Evaluating changes of nodules between a former CT scan and a current follow-up CT scan is a routine clinical task, which is typically performed by
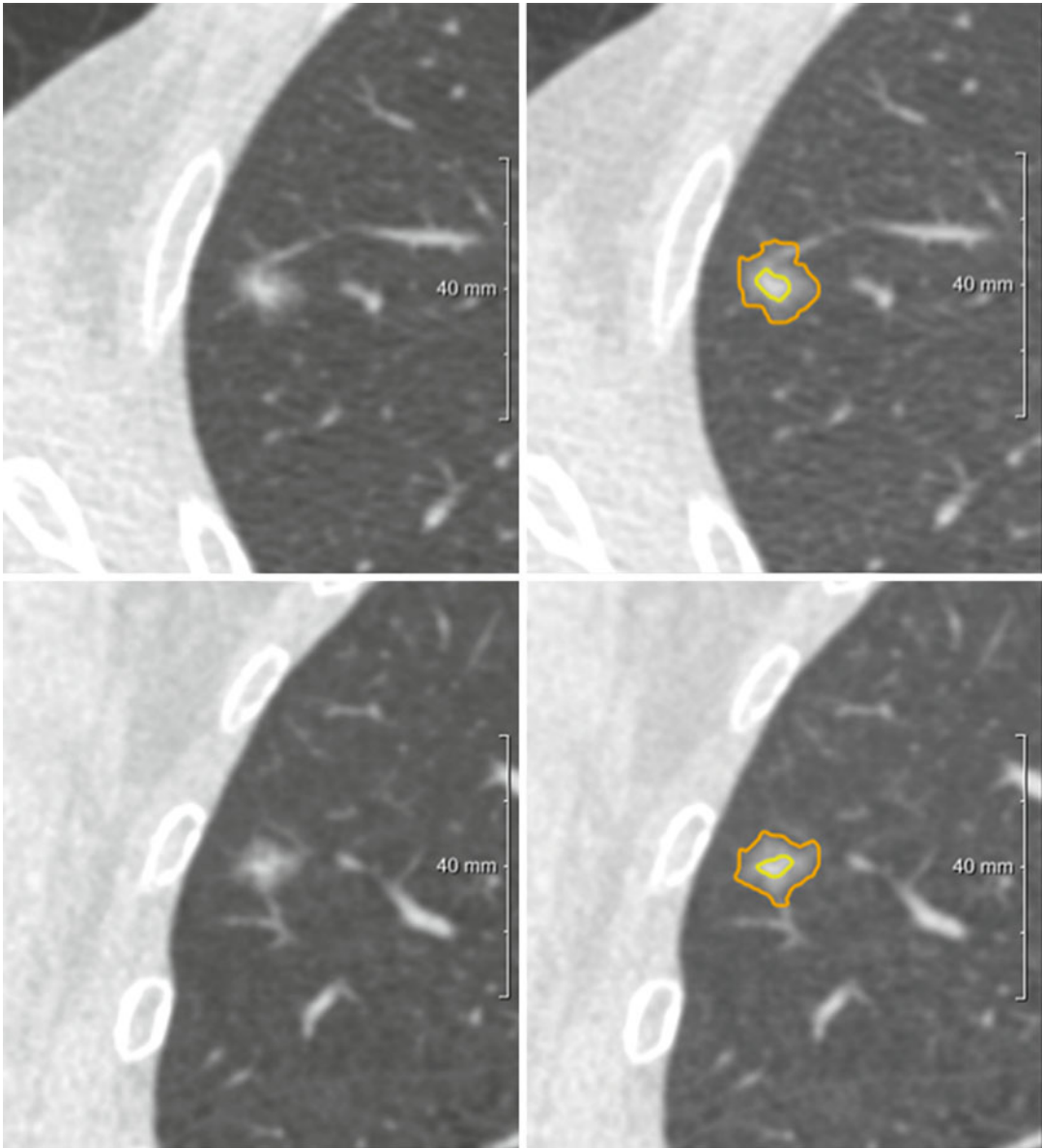
Fig. 6 Axial (*upper*) and coronal (*lower*) CT scans of a part-solid nodule (*left*) and its segmentation results (*right*) separating GGO component from solid component

manual matching of two CT scans requiring large efforts and time. Registration techniques can be applied to improve work efficiency in this task. When two serial CT scans with a 5-mm section thickness in patients with metastatic lung nodules were evaluated, the overall matching rate was 67 % (Lee et al. 2007). Higher matching rate

(82 %) could be achieved on CT scans with a relatively unchanged lung configuration than on CT scans with substantial interval changes (29 %). As the change of lung configuration is small in lung screening settings, the matching rates on screening CT were reported to be 91–93 % (Beigelman-Aubry et al. 2007; Tao et al. 2009).
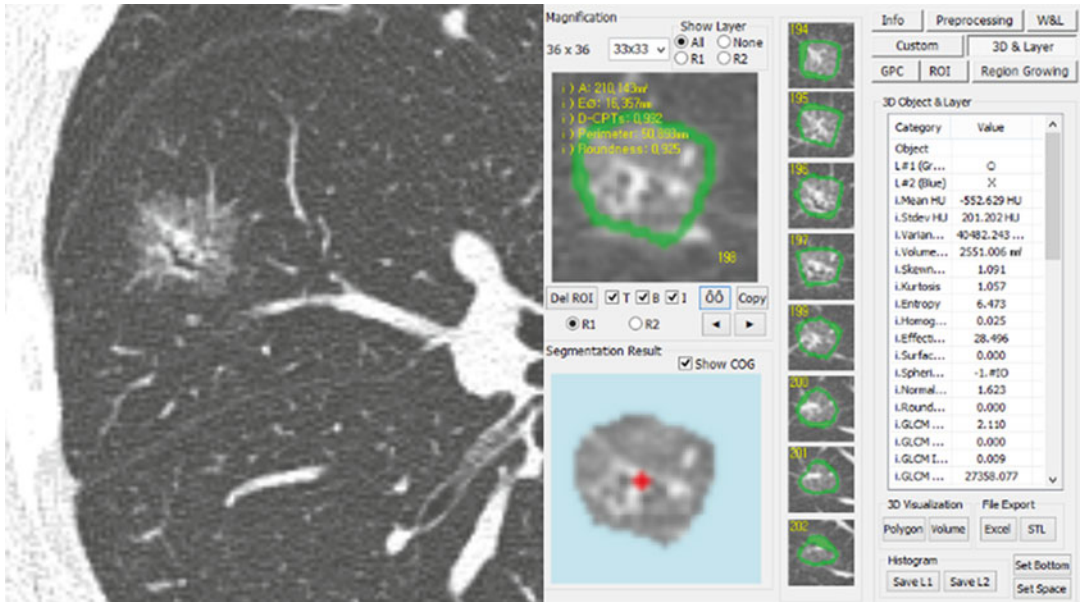
Fig. 7 Texture analysis of subsolid nodule. After segmenting a nodule, various texture features can be calculated as shown in the *right side* table (Courtesy of Park CM, Seoul National University Hospital, Seoul, Korea)

3.6 Role of CAD in Nodule Management

Nodule management in a screening setting usually starts with the assessment to determine the presence or absence of a nodule, the size of nodule, and the attenuation of a nodule whether it is solid, part solid, or pure GGN. Although this looks like a simple approach, considerable variability has been reported among readers. In a study by Jeon et al., the agreement for the positivity of the screening results and follow-up recommendations could be improved from moderate (multirater kappa value, 0.53–0.54) at initial reading to good (multirater kappa value, 0.66–0.67) after reviewing CAD results (Jeon et al. 2012). CAD can be helpful in the classification of lung nodules according to the nodule attenuation. Pairwise agreements for the differentiation between solid nodule, part-solid nodule, and pure GGN were similar between CAD and each of the reader (kappa value, 0.54–0.72) and between readers (kappa value, 0.56–0.81) (Jacobs et al. 2015). The nodule volumetry can also play an important role in lung cancer screening. In the

NELSON trial, the nodule volumetry and estimated volume-doubling time proved to be an effective tool to limit the number of follow-up CT examinations and the overuse of invasive procedures (van Klaveren et al. 2009) (Fig. 8).

4 Chronic Obstructive Lung Diseases

COPD is currently the third most common cause of death in the United States, and mortality from COPD has increased progressively over the last 10 years. As COPD is defined as a disease characterized by persistent airflow limitation caused by the combination of parenchymal destruction (emphysema) and remodeling of the small airways, its diagnosis is made with spirometry. Although pulmonary function tests (PFTs) are reproducible tests and a mainstay in the evaluation of COPD, they represent global measurements of lung function of airways that contribute unequally to airflow. With similar levels of functional impairment, the morphologic manifestations of COPD vary widely. CT can help
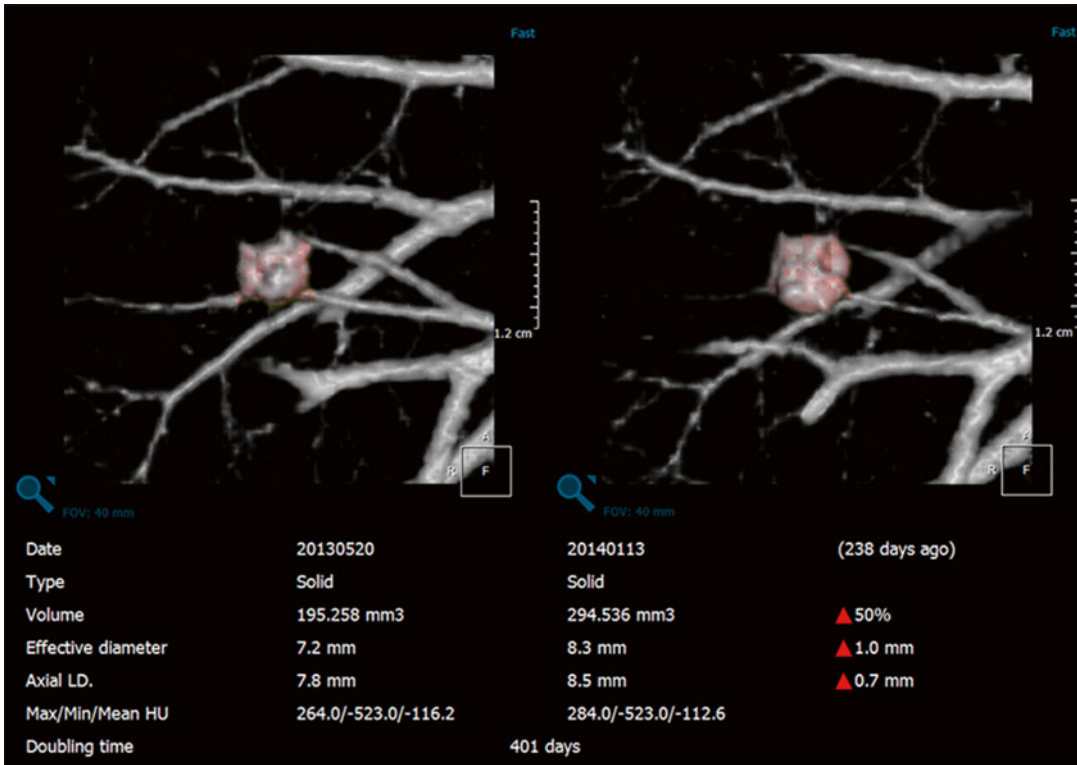
Date	20130520	20140113	(238 days ago)
Type	Solid	Solid	
Volume	195.258 mm3	294.536 mm3	▲50%
Effective diameter	7.2 mm	8.3 mm	▲1.0 mm
Axial LD.	7.8 mm	8.5 mm	▲0.7 mm
Max/Min/Mean HU	264.0/-523.0/-116.2	284.0/-523.0/-112.6	
Doubling time		401 days	

Fig. 8 CT scans obtained at an interval of 238 days shows a growth of a nodule with volume-doubling time of 401 days. This nodule turned out to be lung adenocarcinoma

understanding the heterogeneity of COPD by subphenotyping it into emphysema, large airway abnormality, and small airway obstruction.

Conventional CT analyses of COPD consist of visual assessment to determine the presence, characteristics, and extent of emphysema, airway wall thickening, and air trapping. With the vigorous investigations using quantitative CT, chest CT has become an established modality in quantifying emphysema and measuring various airway dimensions and degree of air trapping.

4.1 Quantification of Emphysema

Emphysema, which is an abnormal permanent enlargement of airspaces distal to the terminal bronchioles accompanied by destruction of alveolar walls, results in replacing the normal lung parenchyma with air-containing spaces.

Therefore, areas of emphysema appear as hypoattenuated areas on CT.

Densitometric analysis for the quantification of emphysema was first introduced by Müller et al. (1988), which is based on a frequency distribution curve of voxels in the lung parenchyma according to CT attenuation coefficients (Yoon et al. 2013) (Fig. 9). Through a series of correlation studies between CT measurements and histology, threshold values representing areas of emphysema have been suggested. Although CT thresholds set at −960 HU or 970 HU showed the highest correlation with histologic emphysema (Madani et al. 2006), the threshold of −950 HU is more commonly used in the interests of balancing sensitivity and specificity (Heussel et al. 2009; Coxson et al. 2013; Regan et al. 2010) (Fig. 10). This measure is usually expressed as emphysema index, percentage of low attenuation area (%LAA), or relative area (RA) of the lung. The size and number of LAA clusters can be
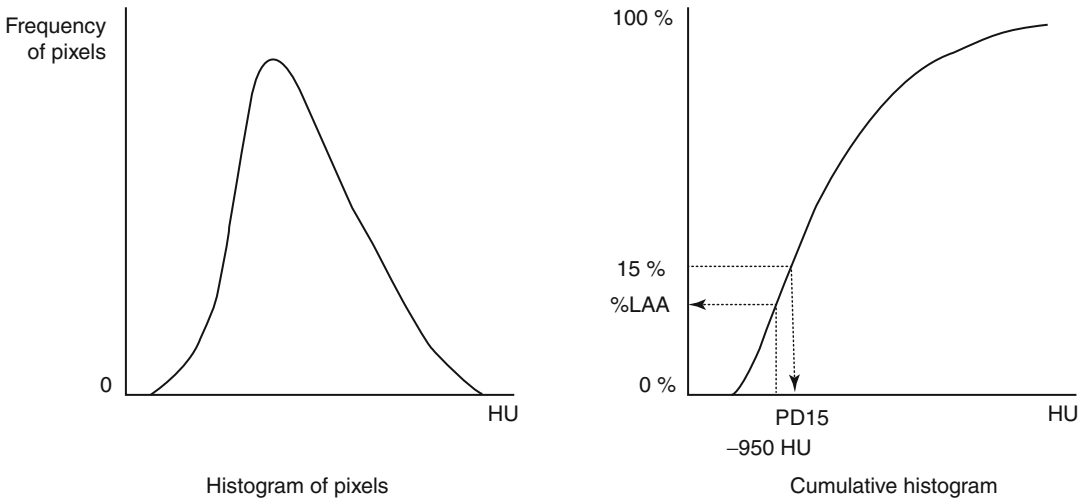
Fig. 9 After segmenting the lung, all the pixels can be plotted according to the attenuation of the pixels resulting in a histogram of pixels. This can be converted to a cumulative histogram, which can be used to calculate %LAA for a specific threshold or a percentile density corresponding to a specific percentile of the lung
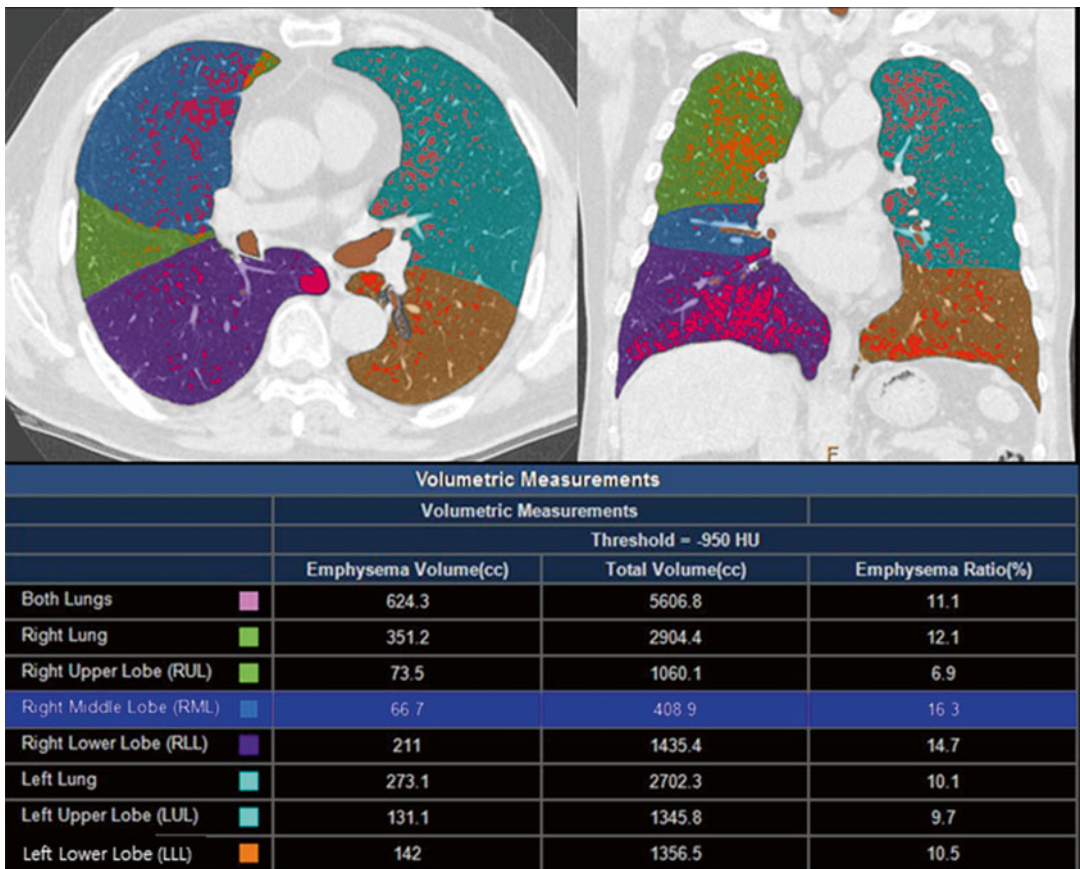

Volumetric Measurements			
Volumetric Measurements			
Threshold = -950 HU			
	Emphysema Volume(cc)	Total Volume(cc)	Emphysema Ratio(%)
Both Lungs	624.3	5606.8	11.1
Right Lung	351.2	2904.4	12.1
Right Upper Lobe (RUL)	73.5	1060.1	6.9
Right Middle Lobe (RML)	66.7	408.9	16.3
Right Lower Lobe (RLL)	211	1435.4	14.7
Left Lung	273.1	2702.3	10.1
Left Upper Lobe (LUL)	131.1	1345.8	9.7
Left Lower Lobe (LLL)	142	1356.5	10.5

Fig. 10 Lobe-based analysis of LAA showing color overlay with red color using a threshold of −950HU. The table shows the volume of LAA (emphysema volume) and the proportion of LAA to the lung volume (emphysema ratio)
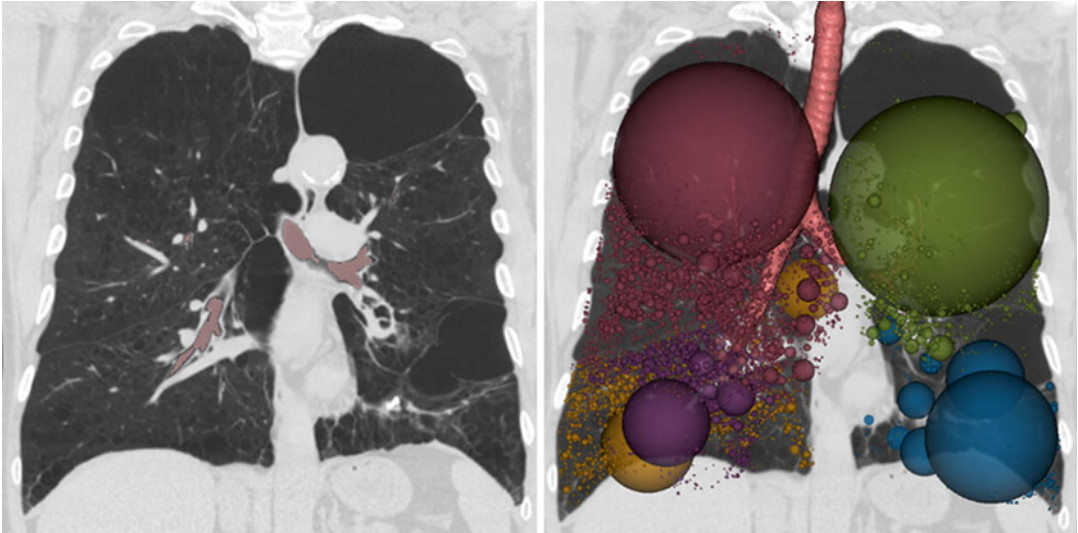
Fig. 11 Coronal CT (*left*) showing extensive emphysema and 3-D representation (*right*) for an index of the size of the low-attenuation clusters (Courtesy of Jin GY, Chonbuk National University Hospital, Jeonju, Korea)

calculated by grouping adjacent low-attenuation voxels together (Fig. 11). With progression of disease, the LAA clusters decrease in number but increase in size, which can be expressed as a fractal dimension, defined as the slope of the cumulative frequency-size distribution of the %LAA (Mishima et al. 1999). Another approach to emphysema quantification is the percentile density method to determine the CT attenuation at a given percentile along the histogram, and the 15th percentile (PD15) is a frequently used point (Fig. 9). A higher PD15 value indicates less emphysema (Heussel et al. 2009; Coxson et al. 2013). The percentile density method approach is reported to be more robust for longitudinal evaluation of emphysema and less sensitive to changes in lung volume (Dirksen 2008).

There are many factors that can affect the quantification of emphysema: lung volume, CT parameters, and status of smoking. When CT scans obtained at 100, 90, 80, 70, and 50 % of vital capacity were evaluated, the %LAA at vital capacity lower than 100 % decreased significantly from that at 100 % vital capacity even though the difference was as small as 2–3 % between 100 % vital capacity and 90 % vital capacity (Madani et al. 2010). Therefore, in CT scanning for emphysema quantification, careful

coaching of respiratory maneuver to patients is essential. Correction for lung volume can also be employed to reduce the variability in longitudinal studies (Stoel et al. 2008; Park et al. 2012). As for CT parameters, section thickness, tube currents, and reconstruction algorithms can affect the quantification. The %LAA can decrease with increasing slice thickness and increasing tube current (Madani et al. 2007). Because the edge-enhancing reconstruction algorithms result in increased %LAA due to increased noise (Boedeker et al. 2004), a standard or smooth reconstruction algorithm is recommended in the emphysema quantification. By applying iterative reconstruction algorithms, the %LAA decreases compared with CT using filtered back projection (Choo et al. 2014). Therefore, standardization of CT parameters and maintaining the same technique are crucial in longitudinal studies. The relationship between the smoking status and %LAA is somewhat paradoxical: lower %LAA in current smokers than in former smokers and increased %LAA after smoking cessation (Grydeland et al. 2009; Ashraf et al. 2011). The potential explanation for these phenomena is that the increase of inflammatory cells in the lung can be caused by smoking and results in increased lung attenuation.
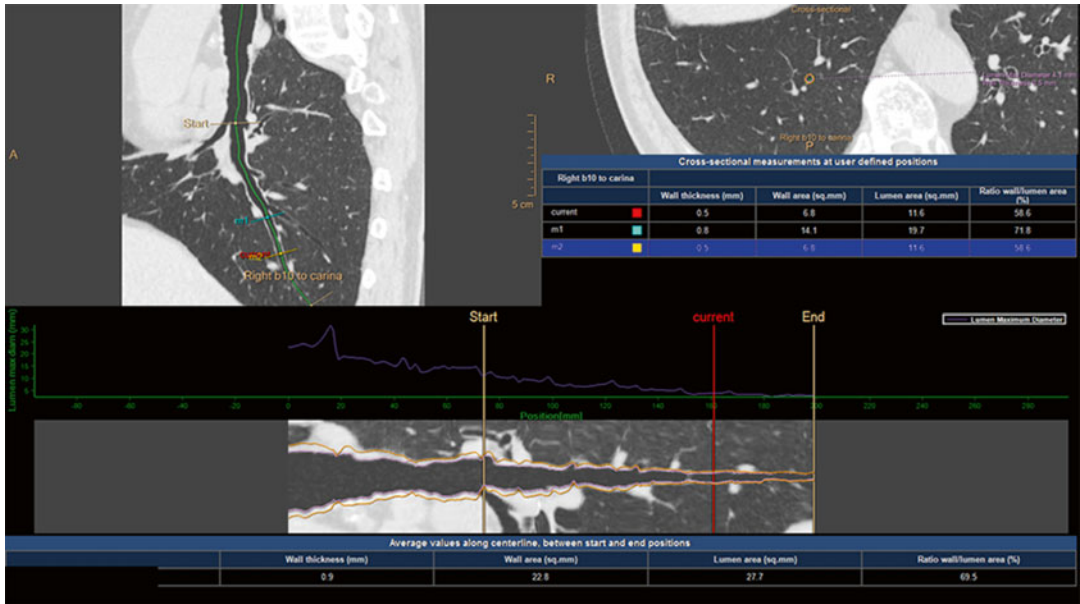
Fig. 12 Curved planar reformation of the bronchial pathway to the right lower lobe (*upper left and bottom*) and orthogonal cross section of the subsubsegmental bronchus in the right lower lobe (*upper right*) show various metrics of airway dimensions

The clinical value of CT quantification of emphysema is that it has close relationship with PFT (Kinsella et al. 1990; Park et al. 1999). Although CT scan in the evaluation of emphysema is usually obtained at inspiration, the %LAA at expiration better reflects PFT than that at inspiration (Kauczor et al. 2002). In addition to the cross-sectional study, CT is now being used for longitudinal studies (Coxson et al. 2013; Regan et al. 2010). In one cohort study which evaluated a longitudinal change over 3 years in 1928 patients with COPD, the annual decline of PD15 was more rapid in women than men and in current smokers than in former smokers, while baseline age, smoking history, airflow limitation, and exacerbation history had no effect (Coxson et al. 2013).

4.2 Measurement of Large Airways

Airway wall remodeling occurs in patients with COPD, and airflow obstruction can be caused by airway wall thickening. These changes on large airways can be seen on CT scan but visual assessment of airway wall thickening is quite subjective. With the increase use of thin-section volumetric chest CT, obtaining various metrics of airway dimensions has become more feasible. Airway luminal area, wall thickness or area, and wall area percent can be calculated to the level of 5th or 6th branches of airways. To produce these measures, after segmenting the airways, a short-axis image is reconstructed in a plane perpendicular to the long axis of the selected airways (Fig. 12). Pi10 is devised to report the summary measures of airways, which is the square root of the wall area of a hypothetical bronchus of internal perimeter 10 mm. This is calculated from the linear regression by plotting the square root of the airway wall area against the internal perimeter of all measured airways (Fig. 13).

Nakano et al. showed that the airway wall area measured at the apical bronchus has an inverse relationship with FEV_1 (Nakano et al. 2000), and subsequent studies on the measurement of airways reported similar results (Berger et al. 2005; Hasegawa et al. 2006). The correlation between

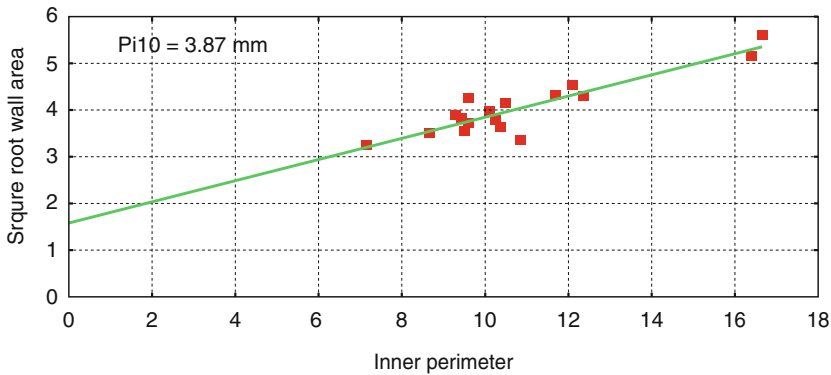|	Average inner Area (mm^2)	Average inner perimeter (mm)	Luminal eccentricity	Average wall thickness (mm)	Wall area (mm^2)	Wall area%
Trachea	280.00	60.15	0.79	2.74	191.02	40.54
LMB	110.06	38.01	0.95	1.89	82.34	42.81
LLB6	77.17	31.92	0.80	1.69	62.55	44.77
LLB	61.96	28.24	0.88	1.75	58.58	48.60
LB10	71.90	32.65	0.56	1.67	46.41	37.21

Fig. 13 Three-dimensional display of the airway with various metrics of airways. A graph at the *bottom* shows how Pi10 was plotted (Courtesy of Jin GY, Chonbuk National University Hospital, Jeonju, Korea)

the airway wall area and airflow limitation tended to be stronger at more distal generations of the bronchi (Hasegawa et al. 2006), and airway wall thickness was larger in smokers with COPD than in smokers or nonsmokers without COPD (Berger et al. 2005). Although the direct measurement of small airways is not feasible or shows large errors, as there is a significant association between the dimensions of the small and large airways, the measurement of the large airways on CT may be used in estimating the changes in the small airways (Nakano et al. 2005).
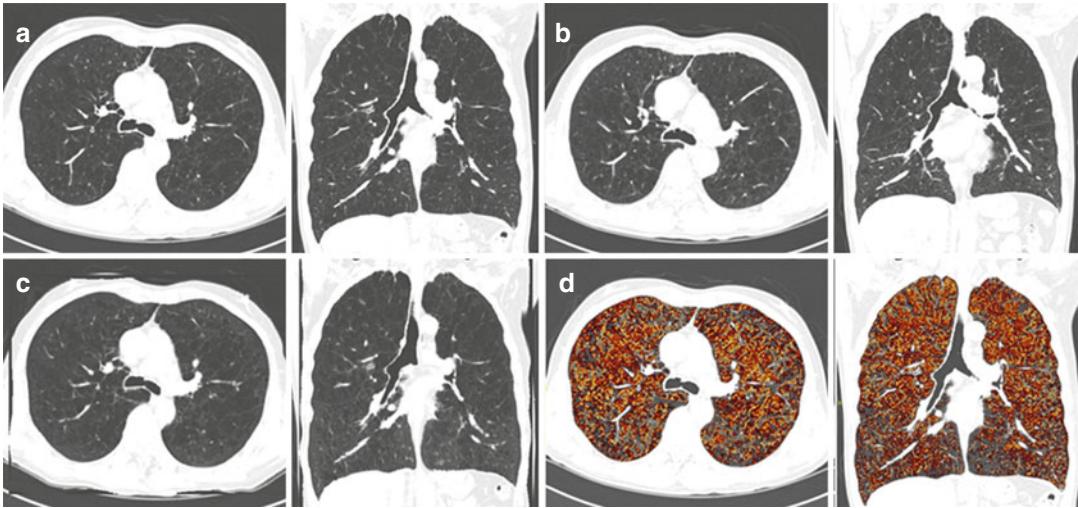
Fig. 14 CT scans obtained at inspiration (**a**) and at expiration (**b**) are used to generate deformed expiration CT images (**c**) with registration techniques. By subtraction of inspiratory CT and deformed expiratory CT, an air-trapping subtraction map (**d**) can be generated (Courtesy of Seo JB, Asan Medical Center, Seoul, Korea)

4.3 Assessment of Small Airway Disease

Small airways are airways with a diameter of 2 mm or less and the main sites of airflow obstruction in COPD. If we consider measurement errors, direct measurement of the wall or lumen of these airways is beyond the range of spatial resolution of current chest CT. Therefore, visual assessment of small airways on CT is based on the indirect findings of air trapping on expiratory CT scan obtained at functional residual capacity or at residual volume. On the other hand, a quantitative analysis of air trapping is challenging, and attenuation-based techniques similar to the quantification of emphysema have been proposed by applying a threshold of −856 or 850 HU at expiratory CT (Regan et al. 2010). The %LAA at expiration shows high correlations with the FEV_1/FVC and with the predicted FEV_1. By combining information of %LAA at inspiration and expiration, COPD subjects may be categorized into predominant emphysema, mixed emphysema and air trapping, and predominant air trapping. Other quantitative approaches for air trapping include the lung volume or attenuation ratio of inspiratory to expiratory CT and the relative volume change of voxels between inspiratory to expiratory CT with attenuation values between −860 HU and −950 HU. The drawback of an attenuation-based technique is that emphysema as well as small airway disease contributes to %LAA of specific thresholds. To overcome this limitation, Galbán et al. proposed a parametric response map which is generated with a voxel-by-voxel co-registration of inspiratory and expiratory CT scans (Galban et al. 2012). Deformable registration is used to spatially align the expiratory scan to the inspiratory scan (Fig. 14) and then classification of voxels in the map into areas of normal parenchyma, small airway disease, and emphysema. This map provides information on the local distribution and extent of COPD phenotypes of small airway disease and emphysema as well as global measures.

5 Diffuse Interstitial Lung Diseases

Impairment of pulmonary function expressed as reduced DLCO and FVC levels is consistently associated with increased mortality in patients with DILD. Although changes in FVC are the most widely used endpoint in drug trials, because of its poor sensitivity to change, it is hard to interpret marginal changes of 5–10 % in an individual (Hansell et al. 2015). Meanwhile,
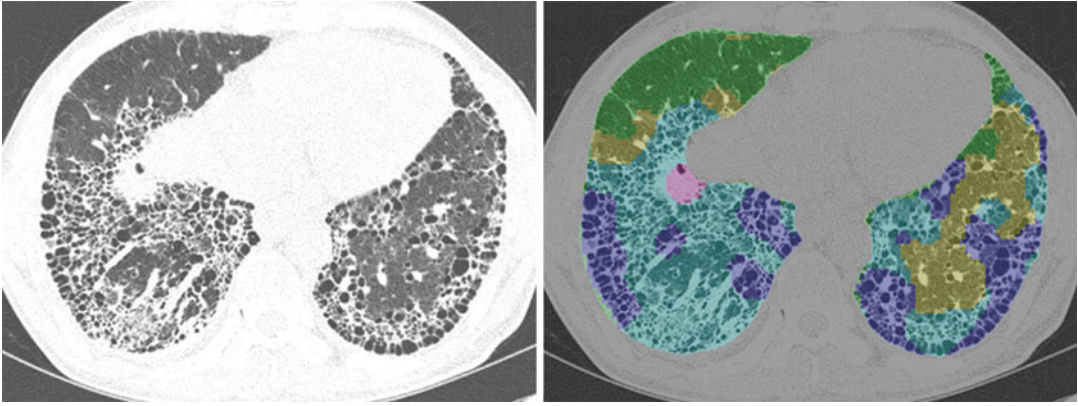
Fig. 15 Transverse CT scan (*left*) and texture-based quantification map (*right*) in a patient with IPF show the areas of different regional patterns expressed as different color overlay on the map: normal (*green*); ground-glass opacity (*yellow*); reticular opacity (*cyan*); consolidation (*pink*); honeycombing (*violet*) (Courtesy of Seo JB, Asan Medical Center, Seoul, Korea)

thin-section CT has been an essential component in making a diagnosis of DILD, but optimal use of CT in monitoring diffuse lung disease was not established. With the recent approval of new drugs by the US Food and Drug Administration for the treatment of idiopathic pulmonary fibrosis (IPF), the quantification of the extent of DILD on CT has become a more important issue (Hansell et al. 2015). In the clinical trials, CT may provide an effective endpoint in addition to PFTs and other biomarkers. Methods to assess disease extent on CT are being investigated from simple visual estimates to sophisticated software quantification. In the past, high-resolution CT scan was obtained with a limited number of thin sections at specific intervals with skipped volume. This approach was employed initially due to limited CT performance, but this technique can be used to reduce radiation exposure to patients. As this non-contiguous imaging is problematic in monitoring disease extent in serial CT scans, contiguous volumetric acquisition of CT is now recommended.

CT findings related with fibrotic interstitial lung diseases are ground-glass opacity, reticular opacity, traction bronchiectasis, and honeycombing. The extent of fibrosis on CT in patients with IPF was reported to be an important predictor of mortality (Lynch et al. 2005). Semiquantitative visual estimation of disease extent has been performed typically on several sections of thin-section CT. However, even among thoracic radiologists, there is considerable variability in defining the presence or absence of these findings (Watadani et al. 2013). Interobserver variability is inevitable in this visual assessment but can be reduced by reader training with standard image references.

5.1 Semiautomated Analysis

A texture-based adaptive multiple feature method was developed to evaluate the lung parenchyma on thin-section CT and showed overall accuracy of 81 % in differentiating four groups of normal subjects and those with emphysema, IPF, or sarcoidosis (Uppaluri et al. 1999). In a study which evaluated the feasibility of automated quantification of regional disease patterns on CT, after training the CAD system by the use of typical ROIs representing patterns of normal, GGO, reticular opacity, honeycombing, emphysema, and consolidation, the overall accuracy of the system in classifying each disease pattern was 89 % (Park et al. 2009) (Fig. 15). When similar approach was employed in evaluating short-term changes in patients with IPF, interval changes in volume of reticular opacity,

total volume of interstitial abnormalities, and % total interstitial abnormalities were predictive of survival after a median follow-up of 2.4 years (Maldonado et al. 2014). This CAD output may be used to generate a composite score which incorporates elements from clinical, radiological, and physiological assessments to predict patients' outcome more effectively than using a single test.

6 Perspective

With the continuous improvement of computer technology, image analyses in future radiology will be more quantitative and more objective using extracted features from images. Although many studies have shown advantages of CAD systems in improving radiologists' performance, the CAD is not widely used as a component of routine clinical practice. While undoubtedly multifactorial, in addition to much room for improvement of CAD performance, a major contributing reason is workflow issue which can be enhanced by seamless incorporation of a CAD system into a PACS environment. Protocol-based sending of CT images to CAD server, preprocessing and generation of CAD results before clinical reading, and robust, easy-to-use manual modification tools for CAD results are a few examples to enhance workflow in the use of CAD. We may use CAD programs consisting of several CAD algorithms targeting different disease entities. For example, a CAD program for low-dose CT scan used in lung cancer screening can be equipped with modules for a lung nodule, COPD, and calcium scoring. By combining the CAD results with the clinical data, prediction models and decision-assistant tools will be available.

To compare CAD results in longitudinal examinations, at the moment it is essential to obtain CT images with the same CT scanner and the same scanning protocol and to analyze with the same version of a CAD program. However, this can be performed only in an ideal research setting and it cannot be applied in daily clinical practice. There can be several measures to reduce measurement variability obtained at non-ideal situations. The use of standardized protocols helps to allow multicenter studies. The vendor should discuss with researchers how the CT outputs across CT vendors can be minimized. Compensation or prediction methods for measurement variability according to various factors may help in comparing quantitative measures obtained in different settings.

References

Armato SG 3rd, McLennan G, McNitt-Gray MF et al (2004) Lung image database consortium: developing a resource for the medical imaging research community. Radiology 232:739–748

Ashraf H, Lo P, Shaker SB et al (2011) Short-term effect of changes in smoking behaviour on emphysema quantification by CT. Thorax 66:55–60

Awai K, Murao K, Ozawa A et al (2006) Pulmonary nodules: estimation of malignancy at thin-section helical CT – effect of computer-aided diagnosis on performance of radiologists. Radiology 239:276–284

Beigelman-Aubry C, Raffy P, Yang W, Castellino RA, Grenier PA (2007) Computer-aided detection of solid lung nodules on follow-up MDCT screening: evaluation of detection, tracking, and reading time. AJR Am J Roentgenol 189:948–955

Berger P, Perot V, Desbarats P, Tunon-de-Lara JM, Marthan R, Laurent F (2005) Airway wall thickness in cigarette smokers: quantitative thin-section CT assessment. Radiology 235:1055–1064

Beyer F, Zierott L, Fallenberg EM et al (2007) Comparison of sensitivity and reading time for the use of computer-aided detection (CAD) of pulmonary nodules at MDCT as concurrent or second reader. Eur Radiol 17:2941–2947

Boedeker KL, McNitt-Gray MF, Rogers SR et al (2004) Emphysema: effect of reconstruction algorithm on CT imaging measures. Radiology 232:295–301

Chae HD, Park CM, Park SJ, Lee SM, Kim KG, Goo JM (2014) Computerized texture analysis of persistent part-solid ground-glass nodules: differentiation of pre-invasive lesions from invasive pulmonary adenocarcinomas. Radiology 273:285–293

Choo JY, Goo JM, Lee CH, Park CM, Park SJ, Shim MS (2014) Quantitative analysis of emphysema and airway measurements according to iterative reconstruction algorithms: comparison of filtered back projection, adaptive statistical iterative reconstruction and model-based iterative reconstruction. Eur Radiol 24:799–806

Coxson HO, Dirksen A, Edwards LD et al (2013) The presence and progression of emphysema in COPD as determined by CT scanning and biomarker expression: a prospective analysis from the ECLIPSE study. Lancet Respir Med 1:129–136

de Hoop B, Gietema H, van Ginneken B, Zanen P, Groenewegen G, Prokop M (2009) A comparison of six software packages for evaluation of solid lung nodules using semi-automated volumetry: what is the minimum increase in size to detect growth in repeated CT examinations. Eur Radiol 19:800–808

de Hoop B, Gietema H, van de Vorst S, Murphy K, van Klaveren RJ, Prokop M (2010) Pulmonary ground-glass nodules: increase in mass as an early indicator of growth. Radiology 255:199–206

Dirksen A (2008) Monitoring the progress of emphysema by repeat computed tomography scans with focus on noise reduction. Proc Am Thorac Soc 5:925–928

Doi K, Giger ML, MacMahon H et al (1992) Computer-aided diagnosis: development of automated schemes for quantitative analysis of radiographic images. Semin Ultrasound CT MR 13:140–152

Galban CJ, Han MK, Boes JL et al (2012) Computed tomography-based biomarker provides unique signature for diagnosis of COPD phenotypes and disease progression. Nat Med 18:1711–1715

Godoy MC, Kim TJ, White CS et al (2013) Benefit of computer-aided detection analysis for the detection of subsolid and solid lung nodules on thin- and thick-section CT. AJR Am J Roentgenol 200:74–83

Goo JM (2011) A computer-aided diagnosis for evaluating lung nodules on chest CT: the current status and perspective. Korean J Radiol 12:145–155

Goo JM, Tongdee T, Tongdee R, Yeo K, Hildebolt CF, Bae KT (2005) Volumetric measurement of synthetic lung nodules with multi-detector row CT: effect of various image reconstruction parameters and segmentation thresholds on measurement accuracy. Radiology 235:850–856

Goo JM, Kim KG, Gierada DS, Castro M, Bae KT (2006) Volumetric measurements of lung nodules with multi-detector row CT: effect of changes in lung volume. Korean J Radiol 7:243–248

Grydeland TB, Dirksen A, Coxson HO et al (2009) Quantitative computed tomography: emphysema and airway wall thickness by sex, age and smoking. Eur Respir J 34:858–865

Hansell DM, Goldin JG, King TE Jr, Lynch DA, Richeldi L, Wells AU (2015) CT staging and monitoring of fibrotic interstitial lung diseases in clinical practice and treatment trials: a Position Paper from the Fleischner society. Lancet Respir Med 3:483–496

Hasegawa M, Nasuhara Y, Onodera Y et al (2006) Airflow limitation and airway dimensions in chronic obstructive pulmonary disease. Am J Respir Crit Care Med 173:1309–1315

Heussel CP, Herth FJ, Kappes J et al (2009) Fully automatic quantitative assessment of emphysema in computed tomography: comparison with pulmonary function testing and normal values. Eur Radiol 19:2391–2402

Jacobs C, van Rikxoort EM, Scholten ET et al (2015) Solid, part-solid, or non-solid?: classification of pulmonary nodules in low-dose chest computed tomography by a computer-aided diagnosis system. Invest Radiol 50:168–173

Jeon KN, Goo JM, Lee CH et al (2012) Computer-aided nodule detection and volumetry to reduce variability between radiologists in the interpretation of lung nodules at low-dose screening computed tomography. Invest Radiol 47:457–461

Kauczor HU, Hast J, Heussel CP, Schlegel J, Mildenberger P, Thelen M (2002) CT attenuation of paired HRCT scans obtained at full inspiratory/expiratory position: comparison with pulmonary function tests. Eur Radiol 12:2757–2763

Kim KG, Goo JM, Kim JH et al (2005) Computer-aided diagnosis of localized ground-glass opacity in the lung at CT: initial experience. Radiology 237:657–661

Kim H, Park CM, Woo S et al (2013) Pure and part-solid pulmonary ground-glass nodules: measurement variability of volume and mass in nodules with a solid portion less than or equal to 5 mm. Radiology 269:585–593

Kinsella M, Muller NL, Abboud RT, Morrison NJ, DyBuncio A (1990) Quantitation of emphysema by computed tomography using a "density mask" program and correlation with pulmonary function tests. Chest 97:315–321

Lee JW, Goo JM, Lee HJ, Kim JH, Kim S, Kim YT (2004) The potential contribution of a computer-aided detection system for lung nodule detection in multidetector row computed tomography. Invest Radiol 39:649–655

Lee KW, Kim M, Gierada DS, Bae KT (2007) Performance of a computer-aided program for automated matching of metastatic pulmonary nodules detected on follow-up chest CT. AJR Am J Roentgenol 189:1077–1081

Lee KH, Goo JM, Park SJ et al (2014) Correlation between the size of the solid component on thin-section CT and the invasive component on pathology in small lung adenocarcinomas manifesting as ground-glass nodules. J Thorac Oncol 9:74–82

Lynch DA, Godwin JD, Safrin S et al (2005) High-resolution computed tomography in idiopathic pulmonary fibrosis: diagnosis and prognosis. Am J Respir Crit Care Med 172:488–493

Madani A, Zanen J, de Maertelaer V, Gevenois PA (2006) Pulmonary emphysema: objective quantification at multi-detector row CT – comparison with macroscopic and microscopic morphometry. Radiology 238:1036–1043

Madani A, De Maertelaer V, Zanen J, Gevenois PA (2007) Pulmonary emphysema: radiation dose and section thickness at multidetector CT quantification – comparison with macroscopic and microscopic morphometry. Radiology 243:250–257

Madani A, Van Muylem A, Gevenois PA (2010) Pulmonary emphysema: effect of lung volume on objective quantification at thin-section CT. Radiology 257:260–268

Maldonado F, Moua T, Rajagopalan S et al (2014) Automated quantification of radiological patterns predicts survival in idiopathic pulmonary fibrosis. Eur Respir J 43:204–212

Marten K, Engelke C, Seyfarth T, Grillhosl A, Obenauer S, Rummeny EJ (2005) Computer-aided detection of pulmonary nodules: influence of nodule characteristics on detection performance. Clin Radiol 60:196–206

Matsumoto S, Ohno Y, Aoki T et al (2013) Computer-aided detection of lung nodules on multidetector CT in concurrent-reader and second-reader modes: a comparative study. Eur J Radiol 82:1332–1337

Mishima M, Hirai T, Itoh H et al (1999) Complexity of terminal airspace geometry assessed by lung computed tomography in normal subjects and patients with chronic obstructive pulmonary disease. Proc Natl Acad Sci U S A 96:8829–8834

Muller NL, Staples CA, Miller RR, Abboud RT (1988) "Density mask". An objective method to quantitate emphysema using computed tomography. Chest 94:782–787

Nakano Y, Muro S, Sakai H et al (2000) Computed tomographic measurements of airway dimensions and emphysema in smokers. Correlation with lung function. Am J Respir Crit Care Med 162:1102–1108

Nakano Y, Wong JC, de Jong PA et al (2005) The prediction of small airway dimensions using computed tomography. Am J Respir Crit Care Med 171:142–146

Oda S, Awai K, Murao K et al (2010) Computer-aided volumetry of pulmonary nodules exhibiting ground-glass opacity at MDCT. AJR Am J Roentgenol 194:398–406

Park KJ, Bergin CJ, Clausen JL (1999) Quantitation of emphysema with three-dimensional CT densitometry: comparison with two-dimensional analysis, visual emphysema scores, and pulmonary function test results. Radiology 211:541–547

Park SO, Seo JB, Kim N et al (2009) Feasibility of automated quantification of regional disease patterns depicted on high-resolution computed tomography in patients with various diffuse lung diseases. Korean J Radiol 10:455–463

Park SJ, Lee CH, Goo JM, Heo CY, Kim JH (2012) Inter-scan repeatability of CT-based lung densitometry in the surveillance of emphysema in a lung cancer screening setting. Eur J Radiol 81:e554–e560

Regan EA, Hokanson JE, Murphy JR et al (2010) Genetic epidemiology of COPD (COPDGene) study design. COPD 7:32–43

Rubin GD, Lyo JK, Paik DS et al (2005) Pulmonary nodules on multi-detector row CT scans: performance comparison of radiologists and computer-aided detection. Radiology 234:274–283

Scholten ET, Jacobs C, van Ginneken B et al (2015) Detection and quantification of the solid component in pulmonary subsolid nodules by semiautomatic segmentation. Eur Radiol 25:488–496

Son JY, Lee HY, Lee KS et al (2014) Quantitative CT analysis of pulmonary ground-glass opacity nodules for the distinction of invasive adenocarcinoma from pre-invasive or minimally invasive adenocarcinoma. PLoS One 9, e104066

Stoel BC, Putter H, Bakker ME et al (2008) Volume correction in computed tomography densitometry for follow-up studies on pulmonary emphysema. Proc Am Thorac Soc 5:919–924

Tao C, Gierada DS, Zhu F, Pilgram TK, Wang JH, Bae KT (2009) Automated matching of pulmonary nodules: evaluation in serial screening chest CT. AJR Am J Roentgenol 192:624–628

Uppaluri R, Hoffman EA, Sonka M, Hunninghake GW, McLennan G (1999) Interstitial lung disease: a quantitative study using the adaptive multiple feature method. Am J Respir Crit Care Med 159:519–525

van Ginneken B, Armato SG 3rd, de Hoop B et al (2010) Comparing and combining algorithms for computer-aided detection of pulmonary nodules in computed tomography scans: the ANODE09 study. Med Image Anal 14:707–722

van Klaveren RJ, Oudkerk M, Prokop M et al (2009) Management of lung nodules detected by volume CT scanning. N Engl J Med 361:2221–2229

Watadani T, Sakai F, Johkoh T et al (2013) Interobserver variability in the CT assessment of honeycombing in the lungs. Radiology 266:936–944

Wormanns D, Kohl G, Klotz E et al (2004) Volumetric measurements of pulmonary nodules at multi-row detector CT: in vivo reproducibility. Eur Radiol 14:86–92

Yanagawa M, Honda O, Yoshida S et al (2009) Commercially available computer-aided detection system for pulmonary nodules on thin-section images using 64 detectors-row CT: preliminary study of 48 cases. Acad Radiol 16:924–933

Yankelevitz DF, Reeves AP, Kostis WJ, Zhao B, Henschke CI (2000) Small pulmonary nodules: volumetrically determined growth rates based on CT evaluation. Radiology 217:251–256

Yoon SH, Goo JM, Goo HW (2013) Quantitative thoracic CT techniques in adults: can they be applied in the pediatric population? Pediatr Radiol 43:308–314

Zhao Y, de Bock GH, Vliegenthart R et al (2012) Performance of computer-aided detection of pulmonary nodules in low-dose CT: comparison with double reading by nodule volume. Eur Radiol 22:2076–2084